(19) Europäisches Patentamt
European Patent Office
Office européen des brevets

(11) EP 1 256 907 A9

(12) **CORRECTED EUROPEAN PATENT APPLICATION**
Note: Bibliography reflects the latest situation

(15) Correction information:
**Corrected version no 1 (W1 A1)**
**Corrections, see page(s) 5, 7, 9, 13, 15, 16**

(48) Corrigendum issued on:
**15.01.2003 Bulletin 2003/03**

(43) Date of publication:
**13.11.2002 Bulletin 2002/46**

(21) Application number: **01000142.8**

(22) Date of filing: **10.05.2001**

(51) Int Cl.[7]: **G06T 5/40**

(84) Designated Contracting States:
**AT BE CH CY DE DK ES FI FR GB GR IE IT LI LU MC NL PT SE TR**
Designated Extension States:
**AL LT LV MK RO SI**

(71) Applicant: **AGFA-GEVAERT**
**2640 Mortsel (BE)**

(72) Inventor: **Dewaele, Piet**
**2640, Mortsel (BE)**

(54) **Retrospective correction of inhomogeneities in radiographs**

(57) Several methods for retrospective correction of intensity inhomogeneites in digital diagnostic radiation images are presented. The methods are based on the correction of a digital image representation by means of a bias field. The bias field is deduced from the digital image representation of the diagnostic radiation image.

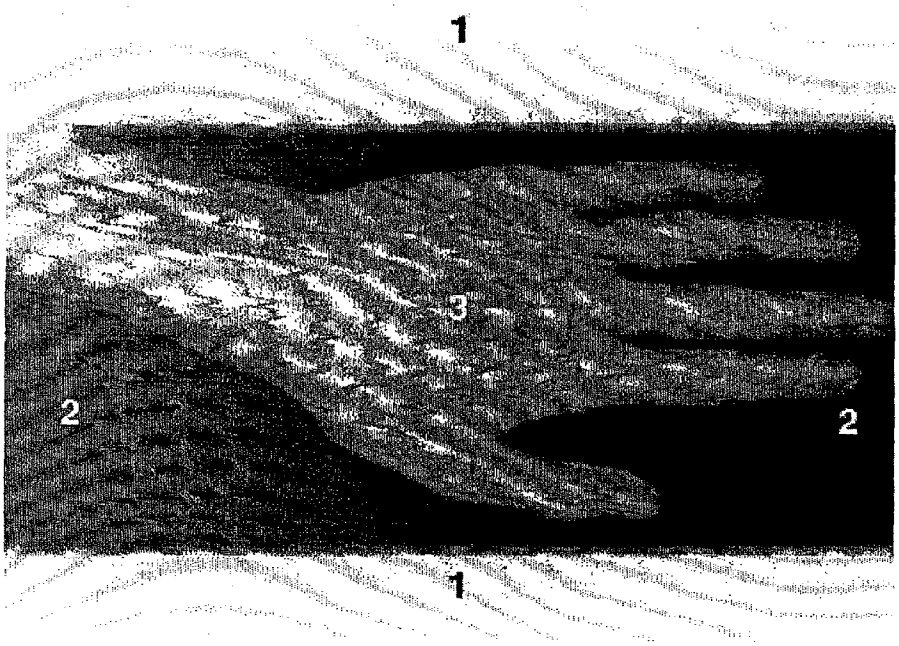


FIG.1

EP 1 256 907 A9

Printed by Jouve, 75001 PARIS (FR)

## Description

FIELD OF THE INVENTION

**[0001]** The present invention relates to a method for correcting inhomogeneities in a digital radiation image which are inherent to the use of a radiation source, a radiation detector or a radiation image read-out apparatus or the like.

BACKGROUND OF THE INVENTION

**[0002]** Digital radiography offers the possibility for computer aided diagnosis and quantitative analysis using image processing techniques such as segmentation, classification and contrast enhancement. However, computer-based image interpretation may be hindered by the presence of the non-uniformities in radiation exposure that are inherent to the image formation.

**[0003]** In the field of X-ray exposure these non-uniformities can be largely attributed to the Heel effect, nevertheless other sources of inhomogeneities exist such as recording member non-uniformities or read-out inhomogeneities.

**[0004]** Although the intensity inhomogeneities induced by all these factors are smoothly varying as a function of location and are easily corrected by the human visual perception system, they complicate the use of automatic processing techniques because the relative brightness of an object within the image becomes position dependent. The overall intensity range is unnecessarily enlarged by the presence of these slowly varying shading components and hence the dynamic range available to represent diagnostic signal details is reduced.

**[0005]** A typical hand radiograph is shown in figure 1. The background at the left side of the image is clearly brighter than at the right side. This phenomenon can be attributed to the so-called Heel effect. Because beam collimator blades substantially attenuate the X-ray beam so as to shield irrelevant body parts, the phenomenon is only visible in the direct exposure and diagnostic areas and not in the collimation area. The Heel effect can be understood from the construction of the X-ray tube as schematically depicted in figure 2. Electrons originating from the cathode are attracted by the positively charged anode. For better heat dissipation, the anode rotates and is inclined by a small anode angle $\theta$, which enlarges the area $A_{actual}$ that is bombarded by electrons while keeping the size of the focal $A_{eff}$, from which rays are projected downward to the object, fairly small. As shown in the diagram of figure 3, this design makes the length of the path travelled by the X-rays through the anode larger on the anode side of the field $T_a$ than on the cathode side $T_c$. Hence the incident X-ray intensity is smaller at the anode side than at the cathode side of the recording device, which explains the inhomogeneity of the background in figure 1.

**[0006]** The Heel effect is one possible cause of intensity inhomogeneities that can be introduced in radiographs. As has already been mentioned higher, other causes of non-uniformities might be envisioned such as non-uniform sensitivity of the recording member, e.g. a photographic film, a photostimulable phosphor screen, a needle phosphor screen, a direct radiography detector or the like. Still another cause might be non-uniformities of the read-out system which is used for reading an image that has been stored in a recording member of the kind described above.

**[0007]** Because the image acquisition parameters that affect intensity inhomogeneity vary from image to image (e. g. variable positioning of the recording device relative to the X-ray source) and can not be recovered from the acquired image at read-out, correction methods based on calibration images or flat field exposure such as the one described in EP-A-823 691 are not feasible.

**[0008]** The method disclosed in EP-A-823 691 comprises the steps of (1) exposing an object to radiation emitted by a source of radiation, (2) recording a radiation image of said object on a radiation-sensitive recording member, (3) reading the image that has been stored in said recording member and converting the read image into a digital image representation, (4) generating a set of correction data and (5) correcting said digital image representation by means of said set of correction data. The set of correction data is deduced from data corresponding with a uniform, flat field exposure of the recording member. The set of correction values represent the deviation of the value that is effectively obtained in a pixel of the recording member and a value that would be expected in the case of flat field exposure. These correction values associated with each recording member are normally determined once and kept fixed during further acquisition cycles.

**[0009]** This type of methods is not applicable for solving problems such as the introduction of inhomogeneities due to the Heel effect.

OBJECTS OF THE INVENTION

**[0010]** It is an object of the present invention to provide a method to correct a digital image for artefacts such as artefacts which are inherent to the use of an X-ray tube, artefacts originating from defects in a radiation detector or the like.

**[0011]** Further objects will become apparent from the description hereafter.

SUMMARY OF THE INVENTION

**[0012]** The above mentioned objects are realised by a method having the specific features set out in claim 1.

**[0013]** Unlike the state of the art methods, in the present invention a set of correction data is deduced from the actual image data obtained by exposing an object to radiation and not from an additional image such as an image representing a flat field exposure.

**[0014]** A radiation image most generally comprises a collimation area which is an area that has been shielded from exposure to radiation by shielding elements, a direct exposure area (also called background area) being the area on the recording member that has been exposed to direct, unmodulated irradiation and a diagnostic area which is the area where the radiation image is found of the body that was exposed to radiation.

**[0015]** Because of substantial attenuation of the X-ray beam when passing through the collimator blades, the dynamic range of the irradiation has been reduced to an extent so as to make these collimation areas unsuitable for estimation of the correction values.

**[0016]** Because the causes that introduce inhomogeneities are not present in the collimation area, the collimation area can be neglected in the method of the present invention. A segmentation algorithm can be used to find the boundaries of the collimation area to exclude these areas from further consideration. An example of such an algorithm has been described in European patent applications EP-A-610 605 and EP-A-742 536 (for the case of a partitioned image), these documents are incorporated by reference.

First embodiment

**[0017]** In one embodiment (1) a mathematical model representing the phenomenon that induces the inhomogeneities is generated. Next (2) the digital image representation is subjected to image segmentation in order to extract data representing an estimation of the direct exposure area. Then , (3) parameters of this model are deduced from image data representing the direct exposure area in the image. Next (4) a bias field is generated on the basis of the deduced parameters. Next, (5) a correction by means of said bias field is applied to the image data. Corrected image data are then subjected to a stopping criterion. Unless this stopping criterion is met, steps (2) to (6) are repeated.

**[0018]** Because the inhomogeneities are only directly measurable in the direct exposure areas of the image, this area is preferably first extracted and the parameters of the model are estimated from the data regarding this region only. A seed fill algorithm can be used to determine the background area. The seed fill algorithm can be started from the boundary of the collimation area.

**[0019]** Inhomogeneity correction by applying a bias field is performed on the entire image. In the context of the present invention the term 'a bias field' is used to denote a low frequency pattern that is superimposed on the average image data values in a multiplicative or additive manner.

**[0020]** Next a new background region is extracted from the corrected image data and the model parameters are re-estimated. This sequence is repeated. The method iterates between background segmentation and correction until convergence, i.e. until no significant changes in background or parameter estimation occur.

Second embodiment

**[0021]** In a second embodiment according to the present invention a statistical model of the image is first generated on the basis of intensity and spatial statistics of image regions in the image.

**[0022]** The digital image representation is then subjected to image segmentation in order to extract data constituting an estimation of these image regions. The image regions referred to are e.g. direct exposure area, bone image, soft tissue image etc.

**[0023]** Parameters of the statistical model are estimated by means of data pertaining to these image regions. Next, a bias field comprising correction data is generated and the entire image is corrected by means of the bias field. The result of the previous step is evaluated relative to a stopping criterion. The method steps of segmenting, bias field correction and evaluation are repeated until the stopping criterion is met. The stopping criterion is e.g. reached when no significant changes occur in the estimation of the image regions and/or no significant changes occur in the parameters defining the statistical model.

**[0024]** In one embodiment the image regions are confined to direct exposure areas. In another embodiment (see fourth embodiment) the method steps are applied separately to each of a number of image region classes jointly constituting the intensity histogram of the radiation image.

**[0025]** In one embodiment the statistical model is a Gaussian distribution and the parameters of the statistical model are the statistical parameters defining the statistical model such as average value $\mu$ of the Gaussian distribution and the standard deviation $\sigma$.

**[0026]** The stopping criterion is e.g. reached when no significant changes occur in the estimation of image regions

and/or no significant changes occur in the parameters defining the statistical model.

Third embodiment

**[0027]** A third embodiment is based on the observation that the entropy of an image increases if inhomogeneities are induced in the image.

**[0028]** In a third embodiment of the method of the present invention an information theoretic model of the image comprising at least direct exposure areas and diagnostic areas is generated. The model is based on Shannon-Wiener entropy increasing when additional intensity value entries are added to the image intensity distribution. The digital image representation is subjected to image segmentation in order to extract data representing an estimation of the direct exposure areas and the entropy in said model is extracted based on of data pertaining to these areas. Next, a bias field is generated and the entire image is corrected by means of the bias field. The result of the previous step is evaluated relative to a stopping criterion and the method is repeated until said stopping criterion is met. A stopping criterion is e.g. met when the entropy is minimal and no significant changes occur in it.

Fourth embodiment

**[0029]** The fourth embodiment is a more general case of the second embodiment. In this fourth embodiment the method steps of the second embodiment are applied separately to each of a number of image region classes jointly constituting the intensity histogram of the radiation image.

**[0030]** In all of the aforementioned embodiments, the number of iterations may be restricted to one when less precision is needed and hence the stopping criterion need not be evaluated.

**[0031]** Further advantages and embodiments of the present invention will become apparent from the following description [and drawings].

BRIEF DESCRIPTION OF THE DRAWINGS

**[0032]**

Fig. 1 shows a typical radiographic image of a hand in which the Heel effect is clearly visible on the direct exposure area,
Fig. 2 and 3 are schematic side views of an X-ray tube,
Fig. 4 is a coordinate system wherein an X-ray originates at position (0,0) and travels along *R* to the recording medium at position *(p, $D_{is}$)*.

DETAILED DESCRIPTION OF THE INVENTION

***First embodiment***

**[0033]** A mathematical model for the Heel effect can be derived from the simplified one-dimensional model of the anode and beam geometry depicted in Fig. 4. In the coordinate system *(p,z)*, with *p* along the anode-cathode axis and *z* along the vertical direction, the X-rays can be taught off to originate within the anode at point ω(0,0), at a distance $D_{ave}$ from the anode surface *S*. Consider the ray *R* at an angle φ from the vertical within the plane (ω,*S*) that hits the recording device at point ($p$,$D_{is}$) with $D_{is}$ the distance between the X-ray source and the recording device and $\tan\phi=\frac{P}{D_{is}}$. The distance *r* traveled by *R* through the anode is given by

$$r=|\xi-\omega|=\sqrt{p_R^2+z_R^2} \tag{1}$$

with $\xi(p_R,z_R)$ the intersection of *R* with *S* which can be found by solving the system of equations:

$$\begin{aligned} S&: p_R = D_{ave} - \tan\theta.z_R \\ R&: p_R = \tan\phi.z_R \end{aligned} \tag{2}$$

**[0034]** Hence,

$$r(p) = D_{ave}\frac{\cos\theta}{\sin(\phi+\theta)} = D_{ave}\frac{\sqrt{1+\left(\frac{p}{D_{is}}\right)^2}}{\tan\theta+\frac{p}{D_{is}}} \quad (3)$$

**[0035]** The radiation received on the recording device is

$$M(p) = I_o.e^{-\mu.r(p)} \quad (4)$$

with $\mu$ the attenuation coefficient of the anode material and $I_o$ the radiation originating at $\omega$.

**[0036]** Model (4) predicts that the Heel effect behaves exponentially along the anode-cathode axis and assumes that it is constant perpendicular to this axis. This is justified by flat field exposure experiments which show that the difference in intensity perpendicular to the anode-cathode axis is relatively small compared to the intensity differences along the anode-cathode axis.

Image segmentation:

**[0037]** A typical hand radiograph, as shown in Fig.1, consists of three regions: collimation area (numeral 1), direct exposure area (numeral 2) and diagnostic regions (numeral 3). Because the Heel effect is largely reduced in the collimation area and directly measurable in the direct exposure area only, the image needs to be segmented to fit model (4) to the image intensity data. This is obtained by first extracting the collimation area and then searching the direct exposure area, the remaining areas being diagnostic regions.

**[0038]** The boundaries of the collimation area have been found using the Hough transform, assuming that these are rectilinear edges as is the case for the majority of X-ray source-mounted collimation devices. To make this approach more robust, the contributions of each image point to the Hough space accumulator are weighted by said point's gradient magnitude and, for each point, only lines the direction of which is within 10 degrees from the normal to the local gradient direction are considered. The 4 most salient points in Hough space that represent a quadragon with inner angles between 80 and 100 degrees are selected as candidate boundaries of the collimation area. Because not all 4 collimation shutter blades leave an imprint in the image and hence make the associated boundaries disappear in the image, candidate boundaries along which the image intensity differs from the intensity expected for the collimation region are rejected.

**[0039]** To extract the background region $B$, a seed fill algorithm has been used that starts from the boundary of the collimation region as determined in the previous step. Appropriate seed points for $B$ are found by considering a small band along each of the collimator edges and retaining all pixels whose intensity is smaller than the mean of the band. This approach avoids choosing pixels that belong to the diagnostic region as candidate seed pixels. $B$ is then grown by considering all neighboring pixels $n_i, i=1,\ldots,8$ of each pixel $p \in B$ and adding $q_i$ to $B$ if the intensity difference between $p$ and $q_i$ is smaller than some specified threshold.

Heel effect estimation:

**[0040]** To fit the model (4) to the image data $N(x,y)$ the direction $\gamma$ has to be found of the anode-cathode axis and the parameters $\alpha = [I_0, \mu, \theta, D_{is}, D_{ave}, p_\omega]$ such that the model best fits the image data within the direct exposure area extracted thus far. $p_\omega$ is a parameter introduced to map point $\omega$ where the X-ray originates to the correct image coordinates (see Fig. 4). For the case whereby the Heel effect is modulated as a one-dimensional phenomenon, the distance $p_\omega$ and the angle $\gamma$ are the required parameters to map the coordinate system attached to the X-ray origin $\omega$ to the image plane coordinate system. However, because the anode has the three-dimensional shape of a cone, the Heel effect is a three dimensional phenomenon, in that the intensity also slightly is reduced in a direction perpendicular to the $(p,z)$ plane. To model the two-dimensional Heel effect in the image plane, a third geometry parameter $p_{\omega\perp}$ is needed. Parameters $(p_\omega, p_{\omega\perp}, \gamma)$ jointly define a coordinate system translation and rotation from the X-ray origin $\omega$ to an image plane origin, which is the center of the image e.g. in practice the Heel effect inhomogeneity in said perpendicular direction is only small with respect to the Heel effect along the anode-cathode axis.

**[0041]** Assuming that $\gamma$ is known, the average image profile $P_\gamma(p)$ along this direction in the direct exposure region $B$ is given by

$$P_\gamma(p) = \langle N(x,y) \rangle_{(x,y)\in B | x.\cos\gamma + y.\sin\gamma = p}$$

with $x$ and $y$ the image coordinates as defined in Fig. 3 and $\langle . \rangle$ the averaging operator. We can then find the optimal model parameters $\alpha^*$ by fitting the expected profile $M(p,\alpha)$ to the measured profile:

$$\alpha^*(\gamma) = \arg\min_\alpha \left\| P_\gamma(p) - M(p,\alpha) \right\| \quad (5)$$

**[0042]** The fitted one-dimensional model $M(p,\alpha^*(\gamma))$ is then back projected perpendicular to the projection axis $\gamma$ to obtain a reconstruction $R(x,y,\gamma,\alpha^*(\gamma))$ for the whole image:

$$R(x,y,\gamma,\alpha^*(\gamma)) = M(x.\cos\gamma + y.\sin\gamma, \alpha^*(\gamma))$$

**[0043]** The direction of the anode-cathode axis $\gamma$ is then determined such that this reconstruction best fits the actual image data within the direct exposure region using

$$\gamma^* = \arg\min_\gamma \left\| N(x,y) - R(x,y,\gamma,\alpha^*(\gamma)) \right\|_{(x,y)\in B} \quad (6)$$

or

$$\gamma^* = \arg\min_\gamma \left\| \frac{N(x,y)}{R(x,y,\gamma,\alpha^*(\gamma))} - 1 \right\|_{(x,y)\in B} \quad (7)$$

depending on whether we wish to use additive or multiplicative correction. The estimated Heel effect is $R(x,y,\gamma^*, \alpha^*(\gamma^*))$ and the corrected image is respectively

$$\hat{N}(x,y) = N(x,y) - R(x,y,\gamma^*\alpha^*(\gamma^*)) \quad (8)$$

or

$$\hat{N}(x,y) = \frac{N(x,y)}{R(x,y,\gamma^*,\alpha^*(\gamma^*))}. \quad (9)$$

**[0044]** The optimal parameters $\alpha^*$ and $\gamma^*$ are found by multidimensional downhill simplex search. It has been noticed that the anode-cathode axis in our setup is almost always parallel to the image or collimation edges. This reduces the number of orientations which have to be evaluated in (6-7) and reduces computation time.

**[0045]** After inhomogeneity correction of the image using (8-9), the direct exposure area $B$ is updated by thresholding, using a threshold derived from the histogram of the corrected image intensities $\hat{N}$. Keeping the previously determined anode-cathode orientation $\gamma$, new values for the optimal model parameters $\alpha^*$ are determined using (5) taking the newly

selected direct exposure region into account. A number of iterations, typically three or four, have been performed between background segmentation and Heel effect correction until convergence.

***Second and third embodiment***

Image formation:

**[0046]** In ideal circumstances, the image formation process of diagnostic digital X-ray images is usually well described by a multiplicative model yielding an intensity-uniform image $U(x,y)$:

$$U(x,y) = I.O(x,y)$$

where $O(x,y)$ represents the object in the image. In diagnostic X-ray images, the most important contributing process of the object is the linear attenuation of the X-rays by the bone and soft tissue

$$O(x,y)=e^{-\int_{\omega}^{\zeta}\mu(r)\,dr}$$

$\mu$ is the linear attenuation coefficient along the path between the origination X-ray at position $\omega$ and the recording device $\zeta$. However, nonuniform illumination $I = I(x,y)$, uneven sensitivity of the recording device and inhomogeneous sensitivity of the phosphors for readout, introduce unwanted intensity modulations in the acquired image $N(x,y)$ described by function $f$

$$N(x,y) = f_{x,y,U}(U(x,y)) \tag{10}$$

**[0047]** In the second and third embodiment the Heel effect is again examined as a very important source of nonuniform illumination. Reference is made to figures 2 - 4 which aid in explaining this effect.

**[0048]** Electrons originating from the cathode are attracted by the positively charged anode. For better heat dissipation, the anode rotates and is inclined by a small anode angle $\theta$, which enlarges the area $A_{actual}$ that is bombarded by electrons while keeping the size of the focal spot $A_{eff}$, from which rays are projected downward to the object, fairly small. As shown in the Fig.3, the design makes the length of the path travelled by the X-rays through the anode larger on the anode side of the field ($T_a$) than on the cathode side ($T_c$). Hence the incident X-ray intensity is smaller at the anode side of the recording device. A simple theoretical model is given by

$$I(x,y)=I_0.e^{-\mu D_{ave}\frac{\sqrt{1+(\frac{p}{D_{is}})^2}}{\tan\theta+\frac{p}{D_{is}}}} \tag{11}$$

with $I_0$ the radiation originating at $\omega$,$\mu$ the linear attenuation coefficient of the anode, $D_{ave}$ the average distance traveled through the anode by the electrons, $D_{is}$ the distance between the X-ray source and the recording device and $p$ the distance from the recording device to X-ray source projected onto the anode-cathode axis.

**[0049]** Although the second and third embodiments are explained with reference to the Heel effect, other source of inhomogeneities may be envisaged such as the moulding process of imaging plates and/or the characteristics of the read-out system. In some fabrication processes, the concentration of phosphors at the edge of the plate is lower than the concentration in the middle of the plate which may result in a non-uniform image. In read-out apparatuses comprising mirror deflection, the displacements of the mirror has to be very accurately implemented to achieve uniform activation of the phosphors for read-out. Due to all these factors, it is almost impossible to model the induced inhomogeneities correctly and more general image formation models are needed.

Problem formulation :

**[0050]** The image formation process is generally modeled with a function $f$ applied to an ideal intensity-uniform image $U(x,y)$, resulting in the acquired image $N(x,y)$. In digital X-ray images, the image degradation process dependency on

the intensity values $U(x,y)$ is relatively small compared to position dependent factors. Hence, we can rewrite equation (10) as follows

$$N(x,y) = f_{x,y}(U(x,y))$$

**[0051]** This equation can be simplified as

$$N(x,y)=U(x,y)S_M(x,y)+S_A(x,y)$$

where $S_M(x,y)$ and $S_A(x,y)$ represent the multiplicative and additive components of the image degradation process. To remove the image inhomogeneities, a corrected image $\hat{U}$ is searched which optimally estimates the true image $U$. If the estimates $\hat{S}_A$ and $\hat{S}_M$ of the actual formation components $S_A$ and $S_M$ are available, the corrected image $\hat{U}$ is given by the inverse of the image formation model

$$\hat{U}(x,y) = \frac{N(x,y)-\hat{S}_A(x,y)}{\hat{S}_M(x,y)}$$

$$= N(x,y)\tilde{S}_M(x,y)-\tilde{S}_A(x,y)$$

$$\text{with } \tilde{S}_M(x,y)=\frac{1}{\hat{S}_M(x,y)} \text{ and } \tilde{S}_A(x,y)=\frac{\hat{S}_A(x,y)}{\hat{S}_M(x,y)} .$$

The problem of correcting the inhomogeneities is thus reformulated as the problem of estimating the additive and multiplicative components $\tilde{S}_A$ and $\tilde{S}_M$.

Correction strategy:

**[0052]** Finding the optimal parameters of the components $\tilde{S}_A$ and $\tilde{S}_M$ involves defining a criterion which has to be optimized. In this section, two criterions are defined.

**[0053]** One correction strategy (second embodiment of the method according to the present invention) is based on the assumption that the intensity values of the direct exposure area (also referred to as background) from the acquired image is Gaussian distributed. In ideal circumstances, this assumption is true for the acquired image $N(x,y)$. The likelihood that a pixel $u_i$ of the corrected image belongs to the background is

$$p(u_i \mid \mu,\sigma)=\frac{1}{\sqrt{2\pi\sigma^2}}\exp\left(-\frac{1}{2}\frac{(u_i-\mu)^2}{\sigma^2}\right) \qquad (12)$$

where $\mu$ and $\sigma^2$ are the true mean and variance of the Gaussian distribution of the background pixels. Given an estimate $\hat{B}$ of the direct exposure area, we seek to maximize the likelihood

$$\prod_{i\in\hat{B}} p(u_i|\mu,\sigma),$$

which is equivalent to minimizing the log-likelihood

$$\hat{U}^* = \arg\min_{\hat{B},\hat{U}} - \sum_{i\in\hat{B}} \log_e p(u_i|\mu,\sigma). \qquad (13)$$

**[0054]** Another embodiment (third embodiment of the method of the present invention) is based on the assumption that the information content of the acquired image is higher than the information content of the uniform image, due to the added complexity of the imposed inhomogeneities:

$$I_c(N(x,y)) = I_c(f_{x,y}U(x,y))) > I_c(U(x,y))$$

**[0055]** The information content $I_c$ can be directly expressed by the Shannon-Wiener entropy

$$I_c(N(x,y)) = H(N(x,y)) = -\sum_n p(n)\log_e p(n) \qquad (14)$$

where $p(n)$ is the probability that a point in image $N(x,y)$ has intensity value $n$. The optimal corrected image $\hat{U}^*$ is thus given by

$$\hat{U}^* = \arg\min_{\hat{U}} H(\hat{U}(x,y)) \qquad (15)$$

Method

**[0056]** Because the Heel effect is almost totally reduced in the collimation area and an estimate of the background $\hat{B}$ is needed to optimize equation (13), a segmentation algorithm is presented.

**[0057]** In the next, implementation details of the correction models of the second and third embodiment of the method according to the present invention are given.

Image Segmentation

**[0058]** The boundaries of the collimation area have been found using the Hough transform, assuming that these are rectilinear edges as is the case for all hand radiographs in our database. To make this approach more robust, the contributions of each image point to the Hough accumulator are weighted by its gradient magnitude and, for each point, only the lines whose direction is within 10 degrees of the normal to the local gradient direction are considered. The 4 most salient points in Hough space that represent a quadragon with inner angles between 80 and 100 degrees are selected as candidate boundary of the collimation area. Because not all 4 collimation boundaries are always present in the image, candidate boundaries along which the image intensity differ from the expected intensity values for the collimation region, are rejected.

**[0059]** To extract the background region $B$, a seed fill algorithm is used that starts from the boundary of the collimation region as determined in the previous step. Appropriate seed points for $B$ are found by considering a small band along each of the collimator edges and retaining all pixels whose intensity is smaller than the mean of the band. This approach avoids choosing pixels that belong to the diagnostic region as candidate seed pixels. The background region is then grown by considering all neighbouring pixels $n_i, i=1,...8$ of each pixel $p\in\hat{B}$ and adding $q_i$ to $\hat{B}$ if the intensity difference between $p$ and $q$ is smaller than some specified threshold.

Maximum likelihood estimation

**[0060]** We simplify (13), by leaving out the multiplicative component $\tilde{s}_M$ of the image degradation process

$$\hat{U}^* = \arg\min_{\hat{B},\hat{U}} - \sum_{i\in\hat{B}} \log_e p(u_i|\mu,\sigma) \qquad (16)$$

$$= \arg\min_{\hat{B},\hat{U}} - \sum_{x,y\in\hat{B}} \log_e p(U(x,y)|\mu,\sigma)$$

$$= \arg\min_{\hat{B},\hat{U}} - \sum_{x,y\in\hat{B}} \log_e p(N(x,y) - \tilde{S}_A(x,y)|\mu,\sigma)$$

**[0061]** This equation is optimized by iteratively estimating the background $\hat{B}$ and finding parameters $\mu$, $\sigma$ and the components $\tilde{s}_A$ after differentation and substitution of $p(u_i|\mu,\sigma)$ by the Gaussian distribution (12). To find the solution for the multiplicative component, the same approach can be followed after logarithmic transforming the intensity values.

**[0062]** The initial estimate for the background $B$ is taken from the segmentation algorithm described higher. All other estimates for $B$ are computed using a histogram based threshold algorithm. The threshold is defined as the smallest value of $\varepsilon$ satisfying

$$\varepsilon^* = \min_{\varepsilon} \bigcap_{i=1,2,3} \left\{ \varepsilon > \mu + \sigma \middle| p_\beta(\varepsilon_\beta) < p_\beta(\varepsilon_\beta + i) \right\}$$

$$\varepsilon_\beta = \left[ \frac{\varepsilon - \min \hat{U}}{\max \hat{U} - \min \hat{U}} \right] 255 \qquad (17)$$

where $p_\beta(n)$ is the probability that a point in image $\hat{U}_\beta$ has value $n$ and $\mu$, $\sigma$ are the mean and variance of the corrected pixels belonging to the previous background estimate.

**[0063]** The maximum likelihood estimates for the parameters $\mu$ and $\sigma$ of 7, can be found by minimization of $-\Sigma_i \log_e p(u_i|\mu,\sigma)$. The expression for $\mu$ is given by the condition that

$$\frac{\partial}{\partial\mu}\left( -\sum_i \log_e p(u_i|\mu,\sigma) \right) = 0.$$

**[0064]** Differentiating and substituting $p(u_i|\mu,\sigma)$ by the Gaussian distribution (12) yields:

$$\mu = \sum_{i \in \hat{B}} \frac{u_i}{n} = \sum_{i \in \hat{B}} \frac{N(x_i, y_i) - \tilde{S}_A(x_i, y_i)}{n}$$

where $x_i, y_i$ is the spatial position of pixel $i$ and $n$ is the number of background pixels. The same approach can be followed to derive the expression for $\sigma$ :

$$\sigma^2 = \sum_{i \in \hat{B}} \frac{(u_i - \mu)^2}{n}$$

$$= \sum_{i \in \hat{B}} \frac{\left(N(x_i, y_i) - \mu \tilde{S}_A(x_i, y_i)\right)^2}{n}$$

**[0065]** Suppose that the spatially smoothly varying component $\tilde{S}_A$ can be modeled by a linear combination of $K$ polynomial basis functions $\phi_j(x_i, y_i)$

$$u_i = N(x_i, y_i) - \sum_{j=1,\ldots,K} c_j \phi_j(x_i, y_i)$$

the partial derivative for $c_k$ of (16) set to zero yields

$$\sum_{i \in \hat{B}} \left[ N(x_i, y_i) - \mu - \sum_j c_j \phi_j(x_i, y_i) \right] = 0 \quad \forall k.$$

**[0066]** Solving this equation for $\{c_j\}$ does not seem very tractable, but combining all equations for all $k$ and introducing matrix notation simplifies the problem considerably

$$C = \begin{bmatrix} c_1 \\ c_2 \\ . \\ . \\ . \end{bmatrix} = AR \qquad (18)$$

where $A$ represents the geometry of the image formation model, each of its rows evaluating one basis function $\phi_K$ at all coordinates and $R$ represents the residue image, i.e. the difference between the acquired image and the estimated background mean. In full matrix notation, the equation is

$$C=\begin{bmatrix}\phi_1(x_1)\,\phi_1(x_2)\,\phi_1(x_3)\ldots\\ \phi_2(x_1)\,\phi_2(x_2)\,\phi_2(x_3)\ldots\\ \cdot\quad\cdot\quad\cdot\quad\ldots\\ \cdot\quad\cdot\quad\cdot\quad\ldots\\ \cdot\quad\cdot\quad\cdot\quad\ldots\end{bmatrix}\begin{bmatrix}n_1-\mu\\ n_2-\mu\\ \cdot\\ \cdot\\ \cdot\end{bmatrix}$$

where $n_i$ is the intensity value of the acquired image at pixel $(x_i,y_i)$. Equation (18) is a least squares fit to the residue image. As least squares fit are sensitive to outliers, only entries in $R$ which satisfy $|n_i-\mu|<2.5\sigma$ are included to solve (18).

Entropy Minimization

**[0067]** Suppose that the image degradation components $\tilde{S}_A$ and $\tilde{S}_M$ can be modeled by a linear combination of $K$ polynomial basis functions $\phi j^{m,a}(x,y)$

$$\tilde{S}_M(x_i,y_i)=\sum_{j=1,\ldots,K_m} m_j\phi_j^m(x_i,y_i)$$

$$\tilde{S}_A(x_i,y_i)=\sum_{j=1,\ldots,K_a} a_j\phi_j^a(x_i,y_i)$$

**[0068]** Equation (15) is reformulated as

$$\{a^*,m^*\}=\arg\min_{a,m}\{H(N(x,y)\tilde{S}_M(x,y)-\tilde{S}_A(x,y))\} \qquad (19)$$

**[0069]** The optimal additive parameters $a^*$ and multiplicative parameters $m^*$ are found by Powell's multidimensional directional set method and Brent's one-dimensional optimization algorithm (W.H. Press, S.A. Teukolsky, W.T. Vetterling, and B.P. Flannery. Numerical Recipes in C. Cambridge University Press, 1992.)

**[0070]** The set of probabilities $p(n)$ in (14) can be obtained by normalization of its histogram. In order to reduce the influence of random effects induced by discretizing the histogram, we use partial intensity interpolation at histogram formation. When transforming the image, an integer intensity value $g$ is transformed to a real value $g'$, which in general lies between two integer values $k$ and $k$+1. The histogram entries $h(k)$ and $h(k+1)$ are updated by $k+1-g'$ and $g'-k$ respectively. To obtain a smoother decline to the absolute minimum and to minimize the effects of local minima, the obtained histogram is blurred to:

$$\hat{h}(n)=\sum_{i=-t}^{t}h(n+i)(t+1-|i|)$$

where the parameter $t$ was set to 3.

Image Formation Models

**[0071]** We have tested different image formation models which are summarized in Table 1. The polynomial models are defined as

$$\phi^{v} = c_0 + c_1 x + c_2 y + c_3 x^2 + c_4 xy + c_5 y^2 + \ldots + c_{\frac{(v+2)!}{2!v!}} y^{v}$$

**[0072]** Models $\Sigma_i, i=1,2$ are included for the maximum likelihood estimation, model $\Sigma_3$ is the general image formation model while model $\Sigma_4$ is derived from (2). Model $\Sigma_5$ is an approximation of model $\Sigma_4$ where the different model parameters are substituted with real values and higher orders are discarded where appropiate. Model $\Sigma_6$ is included for resemblance with model $\Sigma_2$.

Table 1. Image formation models used for correction of inhomogeneities. $\phi^{v}$ is a polynomial model of order $v$.

| Model | Correction |
|---|---|
| $\sum_1^v$ | $\hat{U} = N.\phi^v$ |
| $\sum_2^v$ | $\hat{U} = N + \phi^v$ |
| $\sum_3^v$ | $\hat{U} = N.\phi_1^v + \phi_2^v$ |
| $\sum_4^v$ | $\hat{U} = N.\exp(\frac{\sqrt{\phi_1^v}}{\phi_2^{v-1}})$ |
| $\sum_5^v$ | $\hat{U} = N.\frac{\phi_1^v}{\phi_2^{v-1}}$ |
| $\sum_6^v$ | $\hat{U} = N + \frac{\phi_1^v}{\phi_2^{v-1}}$ |

***Fourth embodiment***

**[0073]** In a fourth embodiment according to the present invention, a statistical mixture model of the image is generated based on a plurality of $K$ image regions.

**[0074]** Each of these regions or classes may physically correspond to e.g. bone, soft tissue and direct exposure area.

**[0075]** In the assumption of a normal mixture model, each class is represented by three unknown parameters: the proportion $\pi_k$ of image pixels, the mean value $\mu_k$ and the variance $\sigma_k^2$.

**[0076]** The set $\psi$ collectively comprising all unknown parameters becomes:

$$\psi = \{\pi_1,...,\pi_K, \mu_1,..., \mu_K, \sigma_1^2,..., \sigma_K^2\}$$

**[0077]** The subset of parameters pertaining to class *k* is denoted as

$$\psi_k = \{\pi_k, \mu_k, \sigma_k^2\}$$

**[0078]** The image intensity histogram, denoting the probability distribution that a pixel *i* has intensity $y_i$ is therefore a Gaussian mixture model

$$f(y_i \mid \psi) = \sum_{k=1}^{K} \pi_k f_k(y_i \mid \psi_k)$$

$$= \sum_{k=1}^{K} \pi_k \frac{1}{\sqrt{2\pi\sigma_k^2}} \exp\left(-\frac{(y_i - \mu_k)^2}{2\sigma_k^2}\right) \qquad i = 1,..., N$$

The basic EM algorithm

**[0079]** The classical analytical method to estimate the parameter $\psi$ is to maximise the log-likelihood function for each of the parameters to estimate.

**[0080]** The maximum likelihood estimates of each parameter can be solved from a system of equations which is non-linear in general and hence requires methods such as Newton-Raphson algorithm.

**[0081]** The Expectation-Maximisation (EM) algorithm estimates the parameters $\psi$ by adding segmentation labels $z_i$ (i represents pixel i and $z_i$ has a value k, k=1 ... K) , (so called non-observable data) to each of the grey values $y_i$ of the pixels (so called observable data).

**[0082]** In each iteration of the EM algorithm the expectation step (E-step) estimates a segmentation label *k* to each pixel *i* on the basis of parameter values $\psi$ from the previous iteration and in the maximisation step (M-step) new parameter values $\psi$ are computed on the basis of maximum likelihood, given the new segmentation labels associated with each of the newly assigned segmentation labels.

The extended EM algorithm

**[0083]** In the context of the present invention two modifications have been added to the EM algorithm to make it correcting for a bias field caused by global inhomogeneities in the imaging chain and to discard outliers due to local inhomogeneities.

**[0084]** The global inhomogeneities in the image distort the assumed normal distribution of the pixel classes.

**[0085]** Every pixel segmentation class is modelled as a normal distribution of which a sum of spatially correlated continuous basis functions is subtracted.

**[0086]** Examples of such basis functions are orthogonal polynomials. Other orthogonal continuous functions may be used as well.

**[0087]** The coefficients of the basis polynomials are added to the parameter set $\psi$ which must be estimated

$$\psi = \{\pi_1,...,\pi_K,\mu_1,...,\mu_K,\sigma_1^2,...,\sigma_K^2,C\}$$

$$= \{\pi_1,...,\pi_K,\mu_1,...,\mu_K,\sigma_1^2,...,\sigma_K^2,c_1,...,c_R\}$$

with the probability distribution for the pixels belonging to segmentation class k

$$f_k(y|\Psi_k C) = \frac{1}{\sqrt{2\pi\sigma_k^2}}\exp\left[-\frac{1}{2\sigma_k^2}\left(y-\mu_k-\sum_{r=1}^{R}c_r\Phi_r\right)^2\right] k=1,...,K$$

with $\phi_r$ a Nx1 vector holding the polynomial function evaluation for the r-th basis polynomial at pixel location i (*i=1...N*).

**[0088]** A further correction to the basic EM algorithm is to make it robust against outliers in the observed distribution of a segmentation class, caused by the presence of local defects (dust, scratch, pixel drop out...) in the recording member, said defects not being attributable to the global inhomogeneities.

**[0089]** To this purpose each pixel class *k* is divided in a Gaussian class (which is distributed by the inhomogeneity and which is corrected by the bias function) and a rejection class. This rejection class is assumed to have a uniform distribution with probability density $\delta_k$ and contains a proportion $\varepsilon\in[0,1]$ of the pixels. The probability distribution of pixel class *k* is therefore

$$f_{k\varepsilon}(y_i|\psi_k) = (1-\varepsilon)f_k(y_i|\psi_k)+\varepsilon\delta_k$$

Summary of the extended EM algorithm

**[0090]** The extended EM algorithm is summarised by the following formulas valid for iteration *m*:

E-step:

**[0091]** For each pixel class *k*, *k=1...K* and each pixel *i*, *i=1...N*, compute

$$p_{ik}^{(m+1)} = \frac{f_k(y_i|\psi_k^{(m)})\pi_k^{(m)}}{\sum_{l=1}^{K}f_l(y_i|\psi_k^{(m)})\pi_l^{(m)}}$$

$$\lambda_k^{(m+1)} = \frac{1}{\sqrt{2\pi\sigma_k^{2(m)}}}\exp(-\frac{1}{2}\kappa^2)$$

$$t_{ik}^{(m+1)} = \frac{f_k(y_i|\psi_k^{(m)})}{f_k(y_i|\psi_k^{(m)})+\lambda_k^{(m+1)}}$$

with

$y_i$ denoting the intensity values of pixel *i*

$\psi_k^{(m)}$ the set of statistical parameter describing class *k* at iteration *m*

$\Pi_k^{(m)}$ the proportion of pixels in the image belonging to class *k* at iteration *m*

$f_k$ the probability density function of intensity of pixels of class k denoting the conditional probability that pixel i has gray value $y_i$ given parameters $\Psi_k$ of class *k*

$p_{ik}^{(m+1)}$ the probability that pixel i belongs to class *k* at iteration *m+1* , these probabilities sum to 1, i.e.

$$\sum_{k=1}^{K} p_{ik}^{(m+1)} = 1 .$$

$\sigma_k^{2(m)}$ the variance of intensity of pixels belonging to class *k* at iteration *m*,

$\kappa$, a threshold on the Mahalanobis distance defined as

$$d_k = \left| \frac{(y_i - \mu_k)}{\sigma_k} \right|$$

$\lambda_k^{(m+1)}$ the probability of pixels of class *k* being outliers,

$t_{ik}^{(m+1)}$ the probability of pixels inside class *k* to belong to the non-rejected group (i.e. not being an outlier). Because $\lambda_k \neq 0$, this probability may be less than one, and hence

$$\sum_{k=1}^{K} p_{ik}^{(m+1)} t_{ik}^{(m+1)} \leq 1 .$$

**[0092]** At this stage, a segmentation of the image could be obtained by a hard classification, i.e. each pixel *i* is assigned class *k* for which $p_{ik}^{(m+1)}$ is maximal, i.e. class pixel

$$i = \arg\max_k \left\{ p_{ik}^{(m+1)} \right\} .$$

In the sequel of the EM algorithm, soft classification labels $p_{ik}^{(m+1)} E[0...1]$ are used.

M-step

**[0093]** For each class *k=1...K* and for each coefficient $c_r$, *r=1...R* applied to the corresponding polynomial basis function , compute

$$\pi_k^{(m+1)} = \sum_{i=1}^{N} \frac{p_{ik}^{(m+1)}}{N}$$

$$\mu_k^{(m+1)} = \frac{\sum_{i=1}^{N} p_{ik}^{(m+1)} t_{ik}^{(m+1)} \left( y_i - \sum_{r=1}^{R} c_r^{(m)} \varphi_{ir} \right)}{\sum_{i=1}^{N} p_{ik}^{(m+1)} t_{ik}^{(m+1)}}$$

$$\sigma_k^{2(m+1)} = \frac{\sum_{i=1}^{N} p_{ik}^{(m+1)} t_{ik}^{(m+1)} \left( y_i - \mu_k^{(m+1)} - \sum_{r=1}^{R} c_r^{(m)} \varphi_{ir} \right)^2}{\sum_{i=1}^{N} p_{ik}^{(m+1)} t_{ik}^{(m+1)}}$$

$$C^{(m+1)} = \begin{bmatrix} c_1^{(m+1)} \\ c_2^{(m+1)} \\ \cdots \\ c_R^{(m+1)} \end{bmatrix} = (A^T W^{(m+1)} A)^{-1} A^T W^{(m+1)} R^{(m+1)}$$

with

$$A = \begin{bmatrix} \varphi_{11} & \varphi_{12} & \cdots & \varphi_{1R} \\ \varphi_{21} & \cdots & & \cdots \\ \cdots & & \cdots & \cdots \\ \varphi_{N1} & \cdots & \cdots & \varphi_{NR} \end{bmatrix}$$

$$W^{(m+1)} = \begin{bmatrix} w_1^{(m+1)} & 0 & \cdots & 0 \\ 0 & w_2^{(m+1)} & & \cdots \\ \cdots & & \cdots & 0 \\ 0 & \cdots & 0 & w_N^{(m+1)} \end{bmatrix}, \quad w_i^{(m+1)} = \sum_{k=1}^{K} \frac{p_{ik}^{(m+1)} t_{ik}^{(m+1)}}{\sigma_k^{2(m+1)}}$$

$$R^{(m+1)} = \begin{bmatrix} y_1 - \tilde{y}_1^{(m+1)} \\ y_2 - \tilde{y}_2^{(m+1)} \\ \cdots \\ y_N - \tilde{y}_N^{(m+1)} \end{bmatrix}, \quad \tilde{y}_i^{(m+1)} = \frac{\sum_{k=1}^{K} \frac{p_{ik}^{(m+1)} t_{ik}^{(m+1)}}{\sigma_k^{2\,(m+1)}} \mu_k^{(m+1)}}{\sum_{k=1}^{K} \frac{p_{ik}^{(m+1)} t_{ik}^{(m+1)}}{\sigma_k^{2\,(m+1)}}}$$

wherein

$\mu_k^{(m+1)}$ denotes the mean intensity value of pixels belonging to class $k$ at iteration $(m+1)$,

$\sigma_k^{2(m+1)}$ denotes the variance of intensity value of pixels belonging to class $k$ at iteration $(m+1)$, after having corrected for the estimate of the bias field,

$C^{(m+1)}$ is a vector containing coefficients $c_r$, $r$=1...$R$ applied to the corresponding polynomial basis function,

$A(i,r)=\phi_{ir}$ is the evaluation of the M-th polynomial basis function at pixel location $i$ (matrix A thus represents the geometry of the bias field model),

$W^{(m+1)}$ is a diagonal matrix of weights $w_i^{(m+1)}$, $i$=1...$N$,

with

$w_i^{(m+1)}$ the weight applied at pixel i in iteration $(m+1)$. Said weight is the sum of the inverse of variance overall classes $k$, $k$=1...K, each weighted with the probability of that class which is $p_{ik}^{(m+1)} t_{ik}^{(m+1)}$.

$R^{(m+1)}$ is a residu image, the residu being the difference between the original image matrix $y_i$, $i$=1...$N$ and the corrected image matrix $\tilde{y}_i^{(m+1)}$ at iteration $(m+1)$.

**[0094]** The equations of the extended EM algorithm reduce to the basic EM algorithm when no bias correction is performed (all $c_r=0$) or no outliers are taken into account (all $\lambda_k=0$ and hence all $t_{ik}=1$).

Initialisation

**[0095]** In order to start the iterations of the EM algorithm, an initial estimate $\psi(0)$ for the parameter set $\psi$ is needed.

**[0096]** This is achieved by assigning each pixel $i$, $i$=1...$N$, to one of the classes $k$=1...$K$ on the basis of intensity histogram slicing.

**[0097]** This assignment involves the computation of $p_{ik}^{(0)}$, which is a hard assignment of probability 1 to one of the $k$ possible class probabilities at pixel $i$ and putting all other probabilities to zero.

**[0098]** Furthermore, no outliers are assumed during initialisation, i.e. $t_{ik}^{(0)}=1$ for all $i$.

**[0099]** Therefor, the M-step in which the values $\psi$ are computed can be executed immediately after initialisation.

**[0100]** Therefore the initialisation step for which the iteration value $m$=0 does not present a true iteration step in the EM algorithm.

**[0101]** To slice the histogram into K distinct initial pixel classes $k$=1...$K$, prior art techniques are used. In the context of the present invention, the histogram is smoothed and approximated with a higher order polynomial, after which the two or three most important maxima are determined. The intensity thresholds separating intensities of different classes are then determined as the intensities corresponding to the minima between these different maxima.

## Claims

1. A method for correction of intensity inhomogeneities in a digital radiation image comprising (1) exposing an object to radiation emitted by a source of radiation, (2) recording a diagnostic radiation image of said object on a radiation-sensitive recording member, (3) reading the diagnostic radiation image that has been recorded on said recording member and converting the read image into a digital image representation, (4) generating a bias field comprising correction data, (5) correcting said digital image representation by means of said correction data, **characterised in that** said bias field is deduced from said digital image representation of said diagnostic radiation image.

2. A method according to claim 1 wherein said digital image representation at least comprises a digital representation

of a direct exposure area and of a diagnostic area and (1) said digital image representation is subjected to image segmentation in order to extract data constituting an estimation of the direct exposure area and an estimation of the diagnostic areas and (2) said set of correction data is deduced from data constituting said estimation of the direct exposure area.

3. A method according to claim 1 wherein said digital image representation at least comprises a digital representation of a direct exposure area and of diagnostic areas and (1) a mathematical model of a cause of said intensity inhomogeneities is generated, (2) said digital image representation is subjected to image segmentation in order to extract data representing an estimation of the direct exposure area, (3) parameters of said mathematical model are deduced from image data corresponding to said direct exposure area, (4) a bias field is generated on the basis of the deduced parameters, (5) said image is corrected by means of said bias field so as to obtain a corrected image, (6) the corrected image is subjected to a stopping criterion, steps (2) to (6) are repeated on the corrected image until the stopping criterion is met.

4. A method according to claim 3 wherein said cause of inhomogeneities is the Heel effect introduced by an X-ray source.

5. A method according to claim 3 wherein said cause of inhomogeneities is the non-uniform sensitivity of a radiation detector.

6. A method according to claim 3 wherein said stopping criterion is met when no significant changes occur in said estimation of the direct exposure area or in the parameters of said mathematical model.

7. A method according to claim 1 wherein (1) a statistical model of said image is generated on the basis of intensity and spatial statistics of image regions in said image, (2) said digital image representation is subjected to image segmentation in order to extract data constituting an estimation of said image regions, (3) parameters of said model are estimated by means of data pertaining to said direct exposure area, (4) a bias field is generated, (5) said image is corrected by means of said bias field, (6) the result of step (5) is evaluated relative to a stopping criterion and steps (2) to (6) are repeated until said stopping criterion is met.

8. A method according to claim 7 wherein said image regions are confined to direct exposure areas.

9. A method according to claim 7 wherein the method steps are applied separately to each of a number of image region classes jointly constituting the intensity histogram of the radiation image.

10. A method according to claim 7 wherein said statistical model is a Gaussian distribution of the direct exposure area and said parameters of the statistical model are the average value $\mu$ of the Gaussian distribution and the standard deviation $\sigma$.

11. A method according to claim 7 wherein said stopping criterion is reached when no significant changes occur in said estimation of image regions and/or no significant changes occur in the parameters defining said statistical model.

12. A method according to claim 1 wherein said digital image representation at least comprises a digital representation of a direct exposure area and of diagnostic areas and (1) an information theoretic model of said image based on Shannon-Wiener entropy is generated, (2) said digital image representation is subjected to image segmentation in order to extract data representing an estimation of the direct exposure area, (3) the entropy in said model is extracted by means of data pertaining to said image regions, (4) a bias field is generated, (5) said image is corrected by means of said bias field, (6) the result of step (5) is evaluated relative to a stopping criterion and steps (2) to (6) are repeated until said stopping criterion is met.

13. A method according to claim 12 wherein said stopping criterion is met when said entropy is minimal and no significant changes occur in the entropy value.

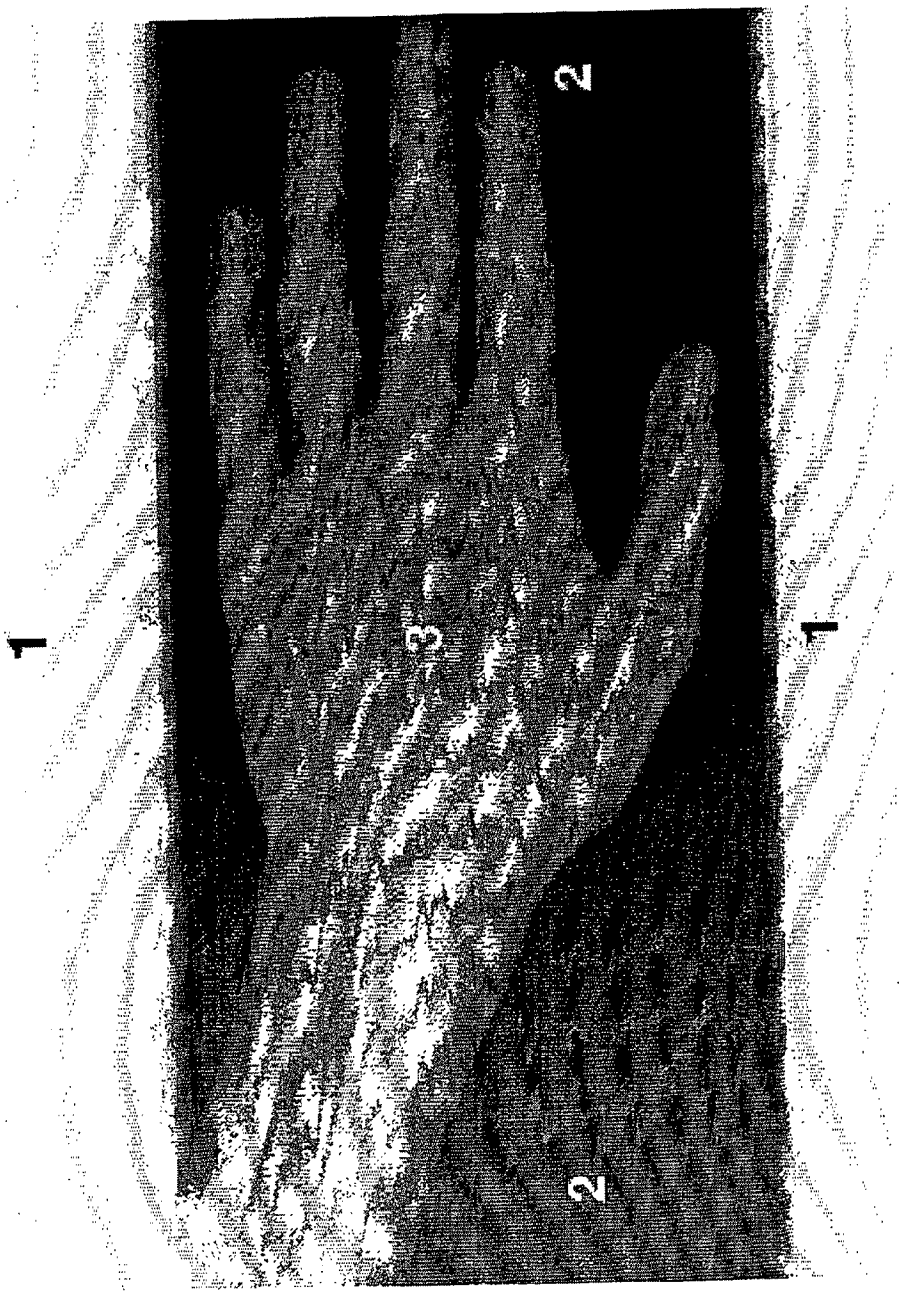


FIG.1

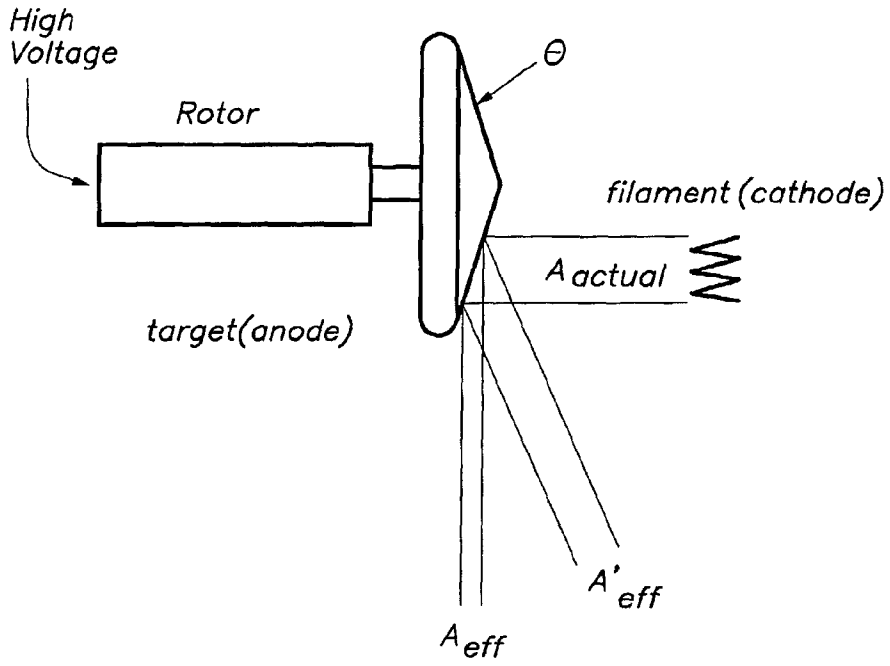
High
Voltage
Rotor
Θ
filament (cathode)
A actual
target(anode)
A'eff
Aeff

FIG. 2

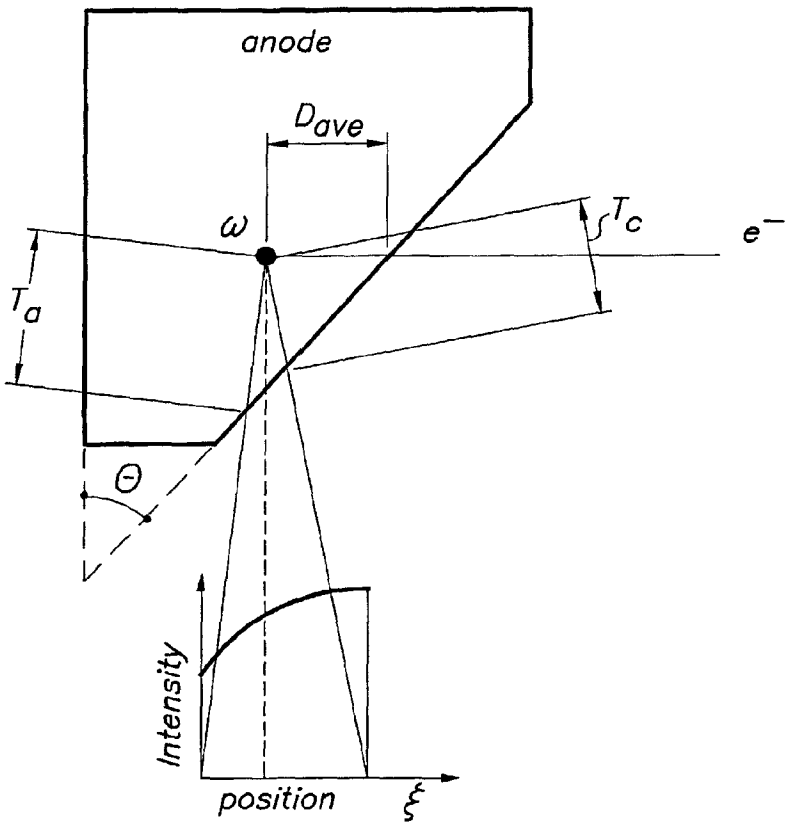


FIG. 3

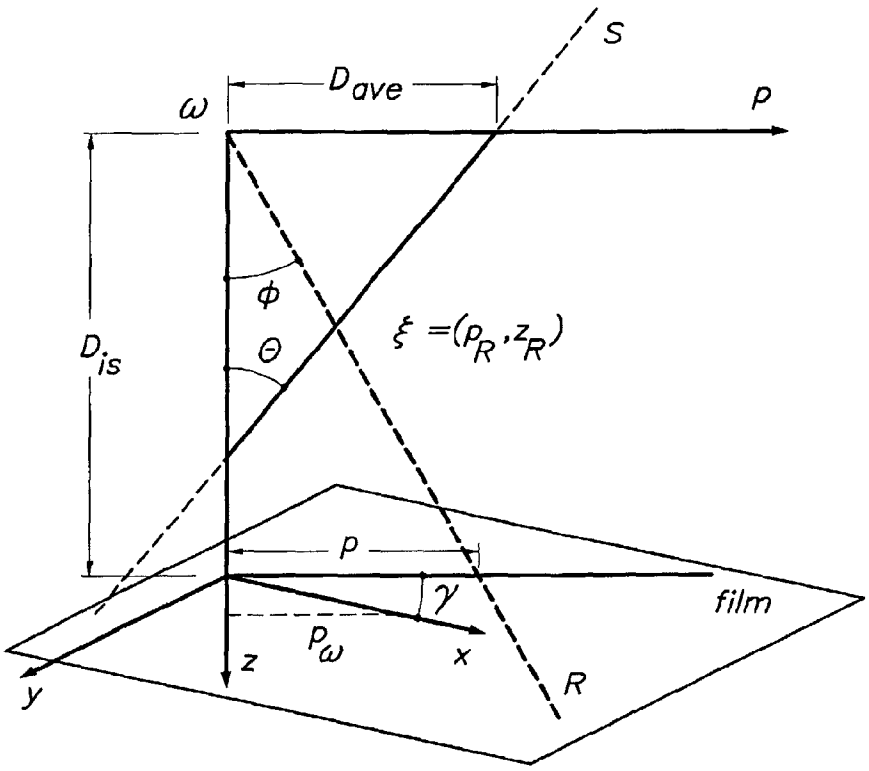


FIG. 4

European Patent Office

# EUROPEAN SEARCH REPORT

Application Number
EP 01 00 0142

## DOCUMENTS CONSIDERED TO BE RELEVANT

| Category | Citation of document with indication, where appropriate, of relevant passages | Relevant to claim | CLASSIFICATION OF THE APPLICATION (Int.Cl.7) |
|---|---|---|---|
| A | US 5 046 118 A (AJEWOLE ISAAC A ET AL)<br>3 September 1991 (1991-09-03)<br>* abstract *<br>* column 3, line 54 - column 5, line 53 *<br>* column 6, line 26 - column 8, line 12 * | 1-13 | G06T5/40 |
| A | US 5 351 306 A (FINKLER KLAUS ET AL)<br>27 September 1994 (1994-09-27)<br>* abstract *<br>* column 2, line 16 - line 45 * | 1-13 | |
| A | EP 0 823 691 A (AGFA GEVAERT NV)<br>11 February 1998 (1998-02-11)<br>* abstract *<br>* page 6, line 4 - line 21 * | 1-13 | |
| A | FURE-CHING JENG ET AL: "INHOMOGENEOUS GAUSSIAN IMAGE MODELS FOR ESTIMATION AND RESTORATION"<br>IEEE TRANSACTIONS ON ACOUSTICS, SPEECH AND SIGNAL PROCESSING, IEEE INC. NEW YORK, US,<br>vol. 36, no. 8,<br>1 August 1988 (1988-08-01), pages 1305-1312, XP000002731<br>ISSN: 0096-3518<br>* page 1305, paragraph II * | 1-13 | TECHNICAL FIELDS SEARCHED (Int.Cl.7)<br>G06T |

The present search report has been drawn up for all claims

| Place of search | Date of completion of the search | Examiner |
|---|---|---|
| THE HAGUE | 17 April 2002 | Gonzalez Ordonez, O |

CATEGORY OF CITED DOCUMENTS

X : particularly relevant if taken alone
Y : particularly relevant if combined with another document of the same category
A : technological background
O : non-written disclosure
P : intermediate document

T : theory or principle underlying the invention
E : earlier patent document, but published on, or after the filing date
D : document cited in the application
L : document cited for other reasons

& : member of the same patent family, corresponding document

EPO FORM 1503 03.82 (P04C01)

## ANNEX TO THE EUROPEAN SEARCH REPORT ON EUROPEAN PATENT APPLICATION NO. EP 01 00 0142

This annex lists the patent family members relating to the patent documents cited in the above-mentioned European search report. The members are as contained in the European Patent Office EDP file on
The European Patent Office is in no way liable for these particulars which are merely given for the purpose of information.

17-04-2002

| Patent document cited in search report | Publication date | Patent family member(s) | Publication date |
|---|---|---|---|
| US 5046118 A | 03-09-1991 | DE 69111932 D1 | 14-09-1995 |
| | | DE 69111932 T2 | 11-04-1996 |
| | | EP 0466907 A1 | 22-01-1992 |
| | | JP 4505228 T | 10-09-1992 |
| | | WO 9112540 A1 | 22-08-1991 |
| US 5351306 A | 27-09-1994 | DE 4129656 A1 | 11-03-1993 |
| EP 0823691 A | 11-02-1998 | EP 0823691 A1 | 11-02-1998 |
| | | JP 10133309 A | 22-05-1998 |
| | | US 5832055 A | 03-11-1998 |

EPO FORM P0459

For more details about this annex : see Official Journal of the European Patent Office, No. 12/82